Infrared study of the phonon modes in bismuth pyrochlores

Minghan Chen and D. B. Tanner
Department of Physics, University of Florida, Gainesville, Florida 32611, USA

Juan C. Nino
Department of Materials Science and Engineering, University of Florida, Gainesville, Florida 32611, USA
(Received 5 January 2005; revised manuscript received 16 May 2005; published 19 August 2005)

The temperature dependence of the reflectance of the cubic bismuth pyrochlores $Bi_{3/2}ZnTa_{3/2}O_7$, $Bi_{3/2}MgNb_{3/2}O_7$, $Bi_{3/2}MgTa_{3/2}O_7$, and $Bi_{3/2}Zn_{0.92}Nb_{1.5}O_{6.92}$ (BZN) has been investigated by infrared spectroscopy. Spectra were collected from 30 to 3300 cm^{-1} between 50 and 300 K, and the optical constants were estimated by Kramers-Kronig analysis and classical dispersion theory. In addition, BZN was studied by terahertz techniques to lower frequencies. Infrared-active phonon modes have been assigned to specific bending and stretching vibrational modes. A previously unassigned infrared mode at $\sim$850 cm^{-1} is discussed. A splitting of the *B*-O stretching phonon modes and O-*B*-O bending modes is assigned to mixed-cation occupancy. The temperature dependence of the phonon frequencies and the damping coefficients are consistent with a decrease of both lattice constant and orientational disorder at low temperatures.

DOI: 10.1103/PhysRevB.72.054303 PACS number(s): 78.30.−j, 63.20.−e

I. INTRODUCTION

Pyrochlores typically have a nominal composition $A_2B_2O_7$ and adopt a cubic structure with space group $Fd3m$. The crystal structure can be described as consisting of interpenetrating networks of BO_6 octahedra and A_2O' chains.[1] The pyrochlore structure allows for a broad range of atomic substitutions at the *A*, *B*, and O sites; therefore, pyrochlore compounds exhibit a wide variety of very interesting physical properties. Recently, bismuth-based pyrochlore compounds have demonstrated excellent properties for use in capacitor and high-frequency filter applications: low loss, high permittivity, and good temperature stability.[2] Golovschikova *et al.*[3] and Jeanne *et al.*[4] first investigated bismuth-based pyrochlore materials for dielectric applications in the early 1970s. Detailed studies by Levin *et al.*[5] determined the stoichiometry of single-phase cubic bismuth zinc niobate to be $Bi_{3/2}Zn_{0.92}Nb_{1.5}O_{6.92}$ (BZN) in the pyrochlore structure ($A_2B_2O_6O'$) with partial Zn occupancy of both *A* and *B* sites. In addition, displacements from the ideal crystallographic positions were identified for both *A* and O′ ions. The *A*-site cations were found to be randomly displaced from the ideal eightfold-coordinated positions along the six ⟨112⟩ directions, perpendicular to the O′-*A*-O′ links. The O′ ions were found to be randomly displaced along the ⟨110⟩ directions. It will be shown that this displacement disorder is required to explain the observed infrared vibrational spectra. Based on crystal chemical considerations, Withers *et al.*[6] determined a range of bond lengths for the *A*-O′ links. Their data indicated that the length of the longer *A*-O′ bond is 2.351 Å while the shorter *A*-O′ bond length is 1.961 Å. The experiment and subsequent Monte Carlo simulation results did provide a good representation of the local short-range order and associated structural relaxation in the A_2O' substructure.

Because vibrational spectroscopy can provide unique information about materials, including phonon modes, the presence of impurities or defects, ordering and the orientation of dipoles, infrared spectra studies of these materials is of great interest. Infrared spectra of pyrochlores were reported by Brisse and Knop.[7] The vibrational modes of stannate pyrochlores were identified, site occupancy was discussed, and trends were analyzed. Later, McCauley[8] studied the general characteristic of infrared absorption in the pyrochlore structure. Factor group analysis was employed, vibrational modes were classified, and infrared-active lattice modes were assigned to specific bending and stretching modes. More recently, Kamba *et al.*[9] measured the reflectance of BZN material and Nino *et al.*[10] assigned each infrared-active mode to a bending or a stretching mode. However, to date, only the spectra of BZN have been reported despite the large number of bismuth-based pyrochlore compounds studied in the last decades. There have been neither studies of the phonon modes in other bismuth pyrochlores nor detailed investigations of the temperature dependence of the infrared absorption in pyrochlores. Here we report temperature-dependent reflectivity measurement for four cubic pyrochlore ceramics $Bi_{3/2}ZnTa_{3/2}O_7$ (BZT), $Bi_{3/2}MgNb_{3/2}O_7$ (BMN), $Bi_{3/2}MgTa_{3/2}O_7$ (BMT), and BZN.

II. EXPERIMENTAL PROCEDURES

Disk-shaped samples with a diameter of 10 mm and thickness of 2 mm were prepared by conventional solid-state powder processing techniques. A detailed description of the process can be found elsewhere.[11] Temperature-dependent reflectivity was obtained using a Fourier transform spectrometer (Bruker IFS 113v) in conjunction with a liquid-helium-cooled Si bolometer (over 30–700 cm^{-1}) and a room-temperature DTGS detector (over 650–3300 cm^{-1}). The reflection stage provided an angle of incidence of about 15° for the light. Temperatures between 50 and 300 K were obtained in a Hanson flow cryostat with polyethylene (far infrared) or KBr windows (midinfrared). Temperature-dependent terahertz transmission spectra of BZN were measured with a Teraview TPI Spectra 1000 spectrometer and a Hanson flow cryostat with polyethylene windows.

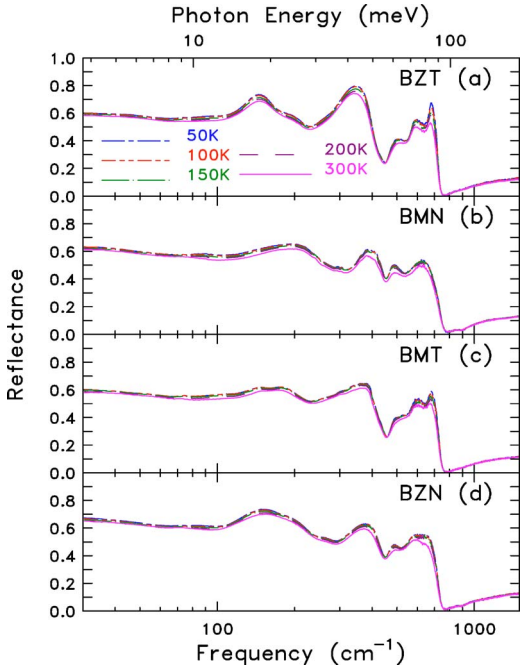

FIG. 1. (Color online) The reflectance of (a) BZT, (b) BMN, (c) BMT, and (d) BZN.

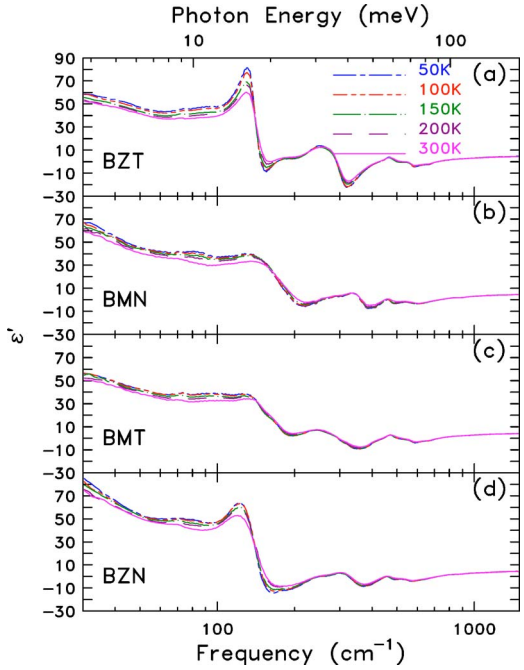

FIG. 2. (Color online) The real part of the dielectric function (ε') of (a) BZT, (b) BMN, (c) BMT, and (d) BZN.

III. RESULTS AND ANALYSIS

A. Reflectance spectra

The temperature-dependent reflectance of BZT, BMN, BMT, and BZN between 30 and 1500 cm^{-1} is shown in Fig. 1. The reflectance is not shown above 1500 cm^{-1} because it is flat at these frequencies, approaching the value given by the high-frequency permittivity ε_∞. Strong structure due to the vibrational modes is seen over much of the range. The low-frequency reflectance is very large, consistent with the large static dielectric constant observed in these materials. The reflectivity spectra do not change significantly with temperature, which implies that there is no phase transition within the temperature range investigated. This is in agreement with earlier infrared measurements of BZN.[12] There is a slight increase in the maxima of the vibrational features at lower temperatures.

B. Kramers-Kronig analysis

The real and imaginary parts of the dielectric constant in the infrared range can be estimated from the reflectance $R(\omega)$ via Kramers-Kronig analysis.[13] In calculating the Kramers-Kronig integral, we extrapolated the reflectance as constant at low frequencies, appropriate for an insulator. At high frequencies we also took the reflectance to be constant up to very high frequencies (10 000 000 cm^{-1}, 12 000 eV) and then used free-carrier behavior $R \sim \omega^{-4}$ above that. Figures 2 and 3 show, respectively, the temperature dependence of the real and imaginary parts of the dielectric function for BZT, BMN, BMT, and BZN. The imaginary part shows a number of peaks due to phonon modes and becomes very small above ~800 cm^{-1}. The real part is quite large (50–60) at low frequencies, shows derivativelike features in the vibrational region, and falls to a high frequency value of about 5.

C. Terahertz spectra

Terahertz transmission spectra of BZN were measured at both room temperature and cryogenic temperature between 3 cm^{-1} and 60 cm^{-1}. The absorption coefficient was estimated from the transmittance and combined with the infrared

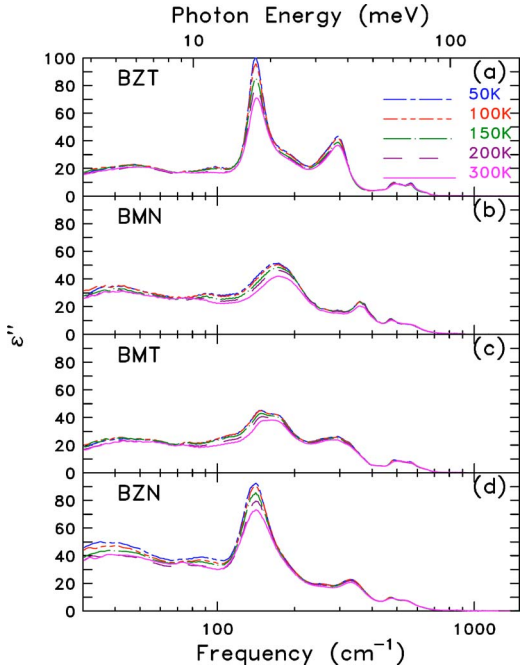

FIG. 3. (Color online) The imaginary part of the dielectric function (ε'') of (a) BZT, (b) BMN, (c) BMT, and (d) BZN.

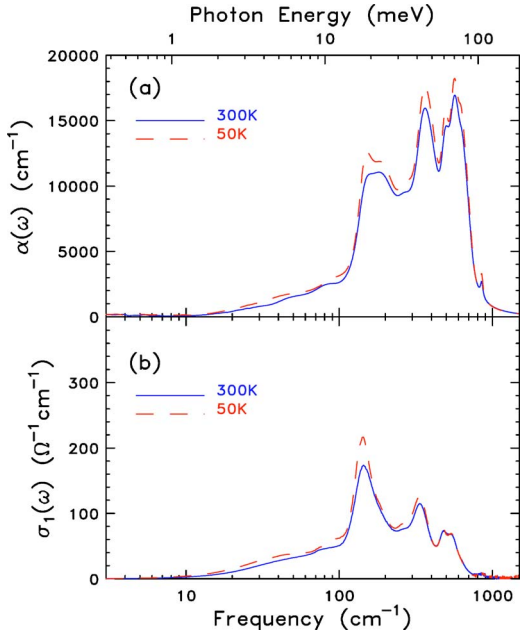

FIG. 4. (Color online) The (a) absorption coefficient and (b) conductivity of BZN at room temperature and at cryogenic temperature.

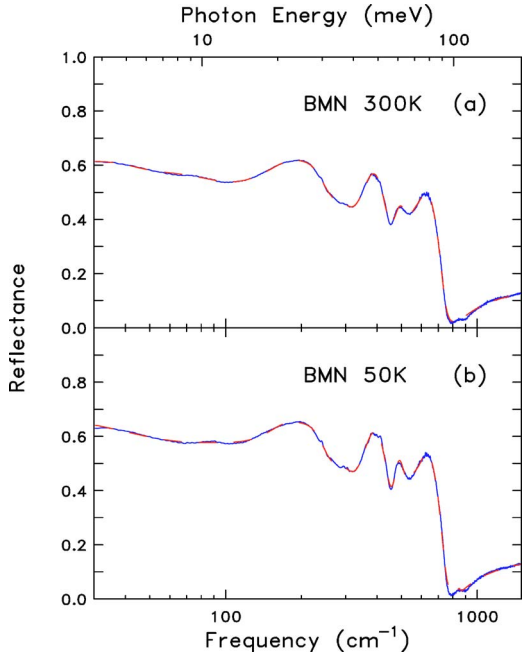

FIG. 5. (Color online) Measured and calculated reflectivity of BMN at (a) 300 K and (b) 50 K.

Kramers-Kronig results to give the absorption coefficient spectra shown in Fig. 4(a) over 3–1500 cm^{-1}. Figure 4(b) shows another optical function, the optical conductivity $\sigma_1(\omega)$. At low frequencies, the optical conductivity decreases, consistent with the small dielectric loss in these materials.

D. Oscillator-model fits

The complex dielectric function $\varepsilon^*(\omega)$ in the infrared range can also be obtained by fitting the reflectance $R(\omega)$ using a model dielectric function that consists of the sum of several damped oscillators plus a high-frequency permittivity ε_∞ originating from the electronic polarization:

$$\varepsilon^*(\omega) = \varepsilon^*_{\text{ph}} + \varepsilon_\infty = \sum_{i=1}^{n} \frac{\Delta\varepsilon_i \omega_i^2}{\omega_i^2 - \omega^2 - j\omega\gamma_i} + \varepsilon_\infty,$$

where ω_i, γ_i, and $\Delta\varepsilon_i$ denote, respectively, the eigenfrequencies, damping coefficient, and contribution to the dielectric permittivity from the ith polar phonon mode and $\varepsilon^*_{\text{ph}}$ is the phonon contribution to the complex dielectric function. The infrared reflectivity spectra and the oscillator fit for BMN measured at room temperature and cryogenic temperature are shown in Fig. 5. The oscillator fits for the other samples are of similar quality. Tables I–IV show the fitting parameters for the reflectance spectra.

IV. DISCUSSION

A. Infrared-active modes

We now turn to assignments of the vibrational features. Factor group analysis of the ideal pyrochlore structure yields[8]

$$\Gamma = 3A_{2u} + 3E_u + A_{1g}(R) + E_g(R) + 4F_{2g}(R) + 8F_{1u}(IR) + 4F_{2u} + 2F_{1g}.$$

Only seven F_{1u} infrared-active modes are infrared allowed. (One F_{1u} mode is an acoustic mode.) However, since as described below, in BZN the atoms in the A sites are displaced from their ideal crystallographic position and occupy one of six equivalent possible positions, and each O′ atom is also displaced among 12 possible positions,[5] the factor group analysis of BZN yields the following phonon modes at the center of the Brillouin zone[9] (assuming some occupancy of all the sites simultaneously, which gives the largest estimate of the expected mode numbers):

$$\Gamma = 2A_{1u} + 6A_{2u} + 2A_{2g} + 8E_u + 5A_{1g}(R) + 7E_g(R) + 13F_{2g}(R) + 15F_{1u}(IR) + 11F_{2u} + 10F_{1g}.$$

The modified irreducible representation was calculated with the refined atomic positions for BZN after Levin *et al.*[5] It is important to note that the overall symmetry of the BZN pyrochlore remains as $Fd3m$. However, as the neutron diffraction experiments show, the A and O′ sites are displaced from their ideal pyrochlore positions (16d and 8b, respectively) to off-center ones (96g and 96g, respectively). While these displacements affect the local symmetry of the atoms and lead to mode splitting due to cation and anion partitioning, the overall unit cell symmetry is kept; i.e., the structure remains a pyrochlore $Fd3m$. Further details are provided in Levin *et al.*[5] In modified irreducible representation, 14 F_{1u} modes are infrared active. (One F_{1u} is an acoustic mode). Ten oscillators are required to fit the infrared reflectivity spectra for BMN and BZN [in agreement with previous work on BZN Ref. 9] and nine modes are needed for BZT and for BMT. Furthermore, similarities in the spectra also suggest possible

TABLE I. Parameters from the dispersion analysis of the phonon modes in the infrared spectra of BZT pyrochlore at 300 and 50 K. An asterisk (*) indicates mode splitting.

300 K				BZT			50 K	
Mode	Resonant frequency ω (cm^{-1})	Oscillator strength $\Delta\varepsilon$	Damping coefficient γ (cm^{-1})	Mode assignment	Resonant frequency ω_n (cm^{-1})	Oscillator strength $\Delta\varepsilon_n$	Damping coefficient γ (cm^{-1})	Mode
ω_7^*	52	15.1	47	(O′-*A*-O′) Bend*	50	16.1	43	ω_7^*
ω_7	86	2.1	29	(O′-*A*-O′) Bend	90	2.9	29	ω_7
ω_6	145	13.3	32	(O-*A*-O) Bend	144	14.8	24	ω_6
ω_5	192	6.0	68	(*A*-BO_6) Stretch	191	9.2	73	ω_5
ω_4	268	3.6	62	(O-*B*-O) Bend	268	3.8	46	ω_4
ω_3	303	4.7	47	(*A*-O) Stretch	303	5.1	38	ω_3
ω_2	499	1.2	81	(*A*-O′) Stretch	496	1.3	72	ω_2
ω_1^*	570	0.78	64	(*B*-O) Stretch*	571	0.86	53	ω_1^*
ω_1	639	0.12	40	(*B*-O) Stretch	640	0.12	30	ω_1
ε_∞	5.24				5.67			
ε (Sum)		47.0				54.2		

analogous *A*-site cation and O′-anion displacements to those observed in BZN.[5,6,9] Assignments of the phonon (lattice) modes are presented in Tables I–IV, following the classification of McCauley[8] and Nino *et al.*[10] Modes identified with an asterisk (*) show a splitting that is inconsistent with the ideal pyrochlore structure, as discussed in more detail below.

B. Mode at 850 cm^{-1}

Both BMN and BZN exhibit a phonon mode around 850 cm^{-1}, identified as ω_n^{**} in Tables II and IV. This feature is seen as a weak structure near the reflectance minimum in Figs. 1(b) and 1(d). In contrast, in the spectra of BMT and BZT this feature is not observed. The room-temperature fits, reported in Tables II and IV, place the ω_n^{**} mode in BMN and BZN at very similar frequencies (850 cm^{-1}). This ω_n^{**} mode shows no significant difference in resonant frequency, oscillator strength ($\Delta\varepsilon$), or damping coefficient (γ) as temperature changes between room temperature and cryogenic temperature. The oscillator strength of this mode (ω_n^{**}) is the smallest among all the lattice modes of both BZN and BMN. McCauley[8] measured the infrared absorption spectra of several pyrochlore-structure materials. The data showed a number of very weak absorption bands in the 800–1100-cm^{-1} region, leading to the suggestion that this lattice mode is an indication of an additional structural complexity As stated before, Withers *et al.*[6] indicated the bond-length difference for the *A*-O′ bond in the A_2O' substructure. Their data show the longer bond length is 2.351 Å and the shorter bond length is 1.961 Å, about a 20% difference. Hector and Wiggin[14] showed that the displacements of both the O′ anion and the *A*-site cation must be cooperative within domains and this may lead to one *A*-O′ bond being shortened and the other being lengthened. According to this picture, the vibration of the shorter *A*-O′ bond may correspond to the phonon mode around 850 cm^{-1} and the vibration of the longer bond may lead to a phonon mode around 483 cm^{-1}.

It has been recently proposed that the disorder of *A* and O′ ions is due to static displacements in all pyrochlores in which the *A* cation has active lone pairs.[15] And it has been noted[16,17] that in some pyrochlores the lone pair character of Bi^{3+} is reduced by mixing of the Bi 6*s* electron pairs and the *d* orbitals (of *B*-site cations). Since Ta has lower electronegativity than Nb, it can be expected that the Bi^{3+} 6*s* electron and *d* orbital (from the *B*-site atom) mixing is stronger in BZT and BMT than that in BZN and BMN. This suggests that in BMT and BZT, the displacement from the symmetrical position of the *A*-site cation and the O′ anions is not as large as in BZN and BMN. In this way, in BMT and BZT, the distinction between the long and short *A*-O′ bonds disappears or it is greatly reduced and, as a consequence, the ω_n^{**} mode is no longer clearly observed.

Furthermore, the phonon mode ω_2 (483 cm^{-1} in BMN and 482 cm^{-1} in BZN), which corresponds to the vibration of the longer A-O′ bond, shifts to higher frequencies (495 cm^{-1} in BMT and 499 cm^{-1} in BZT). At the same time, the ω_n^{**} mode

TABLE II. Parameters from the dispersion analysis of the phonon modes in the infrared spectra of BMN pyrochlore at 300 and 50 K. An asterisk (*) indicates mode splitting. A double asterisk (**) indicates the split *A*-O′ mode described in the present work.

300 K				BMN	50 K			
Mode	Resonant frequency ω (cm^{-1})	Oscillator strength $\Delta\varepsilon$	Damping coefficient γ (cm^{-1})	Mode assignment	Resonant frequency ω_n (cm^{-1})	Oscillator strength $\Delta\varepsilon_n$	Damping coefficient γ (cm^{-1})	Mode
ω_7^*	41	12.4	31	(O′-*A*-O′) Bend*	42	21.6	40	ω_7^*
ω_7	83	19.1	94	(O′-*A*-O′) Bend	108	18.5	126	ω_7
ω_6	178	15.2	84	(O-*A*-O) Bend	173	16.0	73	ω_6
ω_5	211	3.7	79	(*A*-BO_6) Stretch	208	4.6	75	ω_5
ω_4	291	2.0	95	(O-*B*-O) Bend	292	2.3	90	ω_4
ω_3	367	3.6	79	(*A*-O) Stretch	368	3.9	73	ω_3
ω_2	483	0.82	68	(*A*-O′) Stretch	477	0.69	48	ω_2
ω_1^*	556	0.89	108	(*B*-O) Stretch*	548	0.84	99	ω_1^*
ω_1	599	0.35	97	(*B*-O) Stretch	595	0.40	91	ω_1
ω_n^{**}	850	0.01	34	(*A*-O′) Stretch	851	0.01	33	ω_n^{**}
ε_∞	5.44				5.52			
ε (Sum)		58.0				68.9		

would shift to lower frequencies in both BMT and BZT; however, due to its low oscillator strength, the ω_n^{**} mode cannot be detected in the infrared spectrum when it is close to the ω_1 mode.

C. Mode splittings

Not counting the ω_n^{**} mode, BZT, BMN and BZN have in total nine observed infrared modes whereas BMT shows eleven oscillator modes. This difference suggests some additional effects in BMT. The splitting in principle could be due to force-constant or mass effects. Table V shows the mass ratio (the ratio of the mass of the heavier *B*-site ions divided by the mass of the lighter *B*-site ions) of the *B*-site ions for all the compounds investigated. Ta^{5+} has the largest mass of all the *B*-site ions whereas Mg^{2+} is the lightest of all the *B*-site ions. The significant mass difference in BMT leads to a splitting of the *B*-O stretching mode and O-*B*-O bending mode that is large enough to separate the single normal mode into two distinct modes. If we assume that ω_4^* (259 cm^{-1}) and ω_4 (295 cm^{-1}) are the O-*B*-O bending modes in BMT, corresponding to the vibration frequency of Ta^{5+} and Mg^{2+}, respectively, the mass-difference-induced phonon-mode splitting can be explained as follows. We write

$$\omega_p = \sqrt{\Delta\varepsilon}\,\omega_0,$$

$$\omega_P^2 = \frac{4\pi N(Ze)^2}{\mu},$$

where ω_p is the plasma frequency, $\Delta\varepsilon$ is the oscillator strength, μ is the reduced mass of the ions, and (Ze) is the charge of the ions. From the above equations,

$$\mu \propto \frac{(Ze)^2}{\Delta\varepsilon\omega_0^2},$$

so that the reduced mass ratio becomes

$$\frac{\mu_{\mathrm{Ta}}}{\mu_{\mathrm{Mg}}} = \frac{5^2/(\Delta\varepsilon_{\mathrm{Ta}}\,\omega_{\mathrm{Ta}}^2)}{2^2/(\Delta\varepsilon_{\mathrm{Mg}}\,\omega_{\mathrm{Mg}}^2)} = 3.18.$$

In the octahedral structure, the reduced mass can be calculated directly:

$$\mu_{\mathrm{Ta}} = \frac{m_{\mathrm{Ta}}(6m_{\mathrm{O}})}{m_{\mathrm{TA}} + 6m_{\mathrm{O}}},$$

$$\mu_{\mathrm{Mg}} = \frac{m_{\mathrm{Mg}}(6m_{\mathrm{O}})}{m_{\mathrm{Mg}} + 6m_{\mathrm{O}}},$$

where m_{Ta}, m_{Mg}, and m_{O} are the mass of Ta^{5+}, Mg^{2+}, and O^{2-}, respectively, making the reduced mass ratio be

TABLE III. Parameters from the dispersion analysis of the phonon modes in the infrared spectra of BMT pyrochlore at 300 and 50 K. An asterisk (*) indicates mode splitting.

300 K			BMT			50 K	
Mode	Resonant frequency ω (cm^{-1})	Oscillator strength $\Delta\varepsilon$	Damping coefficient γ (cm^{-1})	Mode assignment	Resonant frequency ω_n (cm^{-1})	Oscillator strength $\Delta\varepsilon_n$	Damping coefficient γ (cm^{-1})	Mode
ω_7^*	56	18.8	60	(O′-*A*-O′) Bend*	54	18.0	53	ω_7^*
ω_7	108	4.7	62	(O′-*A*-O′) Bend	110	6.4	54	ω_7
ω_6	149	3.2	35	(O-*A*-O) Bend	145	3.6	27	ω_6
ω_5	178	10.8	71	(*A*-BO_6) Stretch	177	12.1	64	ω_5
ω_4^*	259	3.9	81	(O-*B*-O) Bend	262	5.0	80	ω_4^*
ω_4	295	1.5	50	(O-*B*-O) Bend	299	1.4	42	ω_4
ω_3	336	3.0	79	(*A*-O) Stretch	337	3.1	74	ω_3
ω_2	495	0.73	64	(*A*-O′) Stretch	492	0.77	55	ω_2
ω_1^*	536	0.36	54	(*B*-O) Stretch*	534	0.37	47	ω_1^*
ω_1^*	578	0.60	65	(*B*-O) Stretch*	577	0.64	55	ω_1^*
ω_1	642	0.11	47	(*B*-O) Stretch	644	0.11	36	ω_1
ε_∞	4.98				5.18			
ε (Sum)		47.8				51.5		

$$\frac{\mu_{\mathrm{Ta}}}{\mu_{\mathrm{Mg}}} = 3.23.$$

This result is in agreement with the reduced mass ratio estimated from the oscillator strength. Using this simple spring model, the ratio of the bond strength between different *B*-site ions can be calculated:

$$K \propto \omega^2\mu \Rightarrow K_{\mathrm{Ta}}/K_{\mathrm{Mg}} = \omega_4^{*2}\mu_{\mathrm{Ta}}/\omega_4^2\mu_{\mathrm{Mg}} = 2.49.$$

This result is reasonable. Comparing the radius of the *B*-site ions (sixfold coordinated), one sees that Mg^{2+} and Zn^{2+} have similar radii (0.72 and 0.74 Å, respectively) whereas Ta^{5+} is smaller (0.64 Å).[16] The smaller radius of Ta^{5+} will result in a shorter bond distance and higher bond strength. Thus K_{Ta} is larger than K_{Mg}. In BMN, the material which has the second largest mass ratio, the width of *B*-O stretching mode and O -*B*-O bending mode is rather broad. The large γ values may indicate the contribution by several phonon modes, modes which are too close to appear as individual features in the infrared spectra. In both BZT and BZN, the mass difference at the *B* site is smaller than that of the BMN; correspondingly, the width of O-*B*-O and *B*-O modes is smaller than that of BMN.

Analysis of the *B*-O stretching mode in BMT requires additional considerations. BMT shows only three *B*-O stretching modes instead of the four modes that are expected from mode splitting due to the mass difference. Figure 6 shows this situation. One begins with a single *B*-O stretching mode. The first splitting is due to partial occupancy as well as to the local distortion of the $[BO_6]$ octahedra. The second splitting is due to the mass difference. The two phonon modes which have the central frequencies (midway between 536 and 642 cm^{-1}) are very close to each other and are not separated in the spectrum. Thus the spectrum of BMT only shows a single mode at 578 cm^{-1} with a slightly larger damping coefficient (65 cm^{-1}) than the damping of the other two modes (54 and 47 cm^{-1}, respectively).

D. Low-frequency behavior

The reflectance rises slowly below 100 cm^{-1} (Fig. 1). As made clear by the result of our terahertz transmission measurements (Fig. 4), as well as from the fits to the reflectance, there is a broad vibrational absorption in the range between ~10 and ~100 cm^{-1}. This has been studied in some detail for BZN by Kamba *et al.*[9] At lower frequencies, the optical conductivity decreases to a very small value. These samples

TABLE IV. Parameters from the dispersion analysis of the phonon modes in the infrared spectra of BZN pyrochlore at 300 and 50 K. An asterisk (*) indicates mode splitting. A double asterisk (**) indicates the split *A*-O′ mode described in the present work.

300 K				BZN	50 K			
Mode	Resonant frequency ω (cm^{-1})	Oscillator strength $\Delta\varepsilon$	Damping coefficient γ (cm^{-1})	Mode assignment	Resonant frequency ω_n (cm^{-1})	Oscillator strength $\Delta\varepsilon_n$	Damping coefficient γ (cm^{-1})	Mode
ω_7^*	45	30.8	46	(O′-*A*-O′) Bend*	42	48.8	50	ω_7^*
ω_7	81	10.0	48	(O′-*A*-O′) Bend	88	12.8	57	ω_7
ω_6	142	16.3	41	(O-*A*-O) Bend	142	18.9	34	ω_6
ω_5	178	10.9	84	(*A*-BO_6) Stretch	181	10.2	76	ω_5
ω_4	259	2.3	86	(O-*B*-O) Bend	263	2.8	82	ω_4
ω_3	340	4.9	96	(*A*-O) Stretch	341	5.3	88	ω_3
ω_2	482	0.84	73	(*A*-O′) Stretch	480	0.87	62	ω_2
ω_1^*	551	0.88	90	(*B*-O) Stretch*	550	0.84	74	ω_1^*
ω_1	624	0.08	64	(*B*-O) Stretch	615	0.13	59	ω_1
ω_n^{**}	850	0.01	38	(*A*-O′) Stretch	849	0.02	38	ω_n^{**}
ε_∞	5.24				5.50			
ε (Sum)		77.0				100.7		

are insulators; there is no free-carrier contribution to the conductivity in the measured frequency range. Our estimates of the phonon contribution to the static dielectric constant are in Tables I–IV. Including the high-frequency electronic contribution of around 5, the low-frequency dielectric constants of our samples are between 52 and 106.

E. Temperature effects

In BZT, the ω_7 mode shifts to higher frequencies at low temperature. In BMN, frequency of ω_7 increases significantly at low temperatures. In BZN, ω_7 and ω_4 shift significantly to higher frequencies. In BMT, there is also an increase of the phonon frequency for the ω_4 mode at low temperatures. Figure 7 shows these processes. These phenomena are due to the decrease of the lattice constant on cooling and are consistent with x-ray and neutron diffraction measurements of BZN.[5]

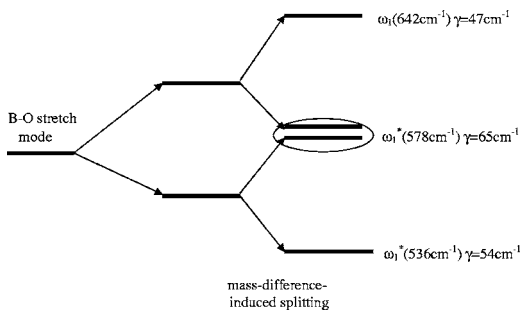

FIG. 6. The splitting of the *B*-O stretching mode in BMT.

The ω_1^*, ω_1, ω_2, and ω_6 modes in BMN and the ω_1 mode in BZN behave differently, shifting to lower frequencies with decreasing temperature. The same is observed in BMT for the ω_6 phonon mode. This behavior probably indicates a more complicated situation controlling these phonon modes. Other phonon modes in these samples do not show significant changes in frequencies at low temperatures.

The widths of phonon modes ω_1, ω_1^*, ω_2, ω_3, ω_4, ω_4^*, and ω_6, decrease with decreasing temperature for all of the samples. The broadening of the phonon mode can be accounted for by structural disorder, orientational disorder, and anharmonicity. Because the widths of these modes are temperature dependent, orientational disorder may play a very important role. Orientational disorder was also found in ti-

TABLE V. The mass ratio of the *B*-site ions in different pyrochlores.

Materials	BMT	BMN	BZT	BZN
Mass ratio	7.444	3.823	2.767	1.421

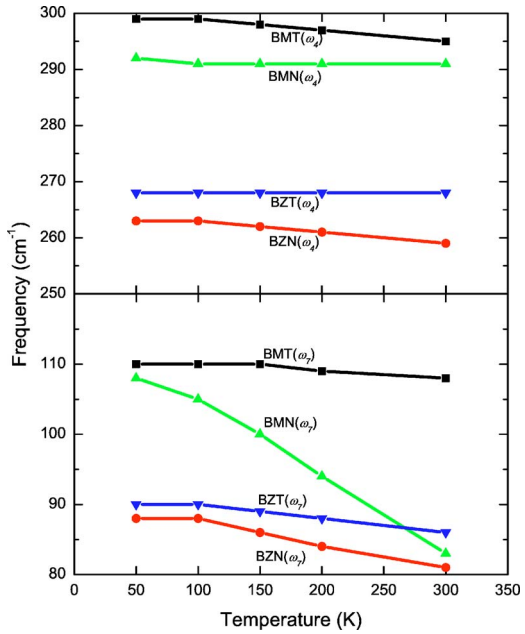

FIG. 7. (Color online) Temperature dependence of the phonon mode frequencies in BZT, BMN, BMT, and BZN.

tanate pyrochlore materials[18] and in bismuth oxide and its derivatives[19] using Raman spectroscopy. The widths of the O-*B*-O (ω_4) and the *B*-O (ω_1^* and ω_1) modes can be explained by the orientational disorder in the BO_6 octahedra. The width of the *A*-O the *A*-O′ stretching modes may be due to the randomization of the orientation of the nonbonding lone pair orbital of Bi^{3+} on the *A* site. This conclusion is in agreement with other experiments.[19]

The variation of the widths for O′-*A*-O′ modes (ω_7^* and ω_7) is not easy to understand. For BMN and BZN, the widths of the ω_7^* and ω_7 modes increase as temperature is reduced. In BMT, the widths of ω_7 and ω_7^* decrease as the temperature is reduced. In BZT, the widths of ω_7^* decrease while the width of the ω_7 mode does not change at cryogenic temperatures. The bending of O′-*A*-O′ bonds, which leads to the separation of the positive- and negative-charge center, creates the dipoles in these materials. The displacement of *A*-site cations and O′ anions might increase the orientation disorder of these dipoles. With the present data, there are no discernible trends in the widths of the ω_7 and ω_7^* modes; consequently, additional spectroscopy in the THz region is needed. Finally, the width of the *A*-BO_6 (ω_5) stretching mode depends on both the orientation of the non-bonding lone pair of *A*-site Bi^{3+} and the orientation of the BO_6 octahedra, and therefore its analysis is not trivial. While the width of ω_5 increases in BZT as the temperature decreases, in BMN, BMT, and BZN it decreases.

V. CONCLUSIONS

Dispersion analyses of the infrared reflectance of BZT, BMN, BMT, and BZN show behavior of the phonon modes which confirms the *A*-site-cation and O′-anion displacement. The assignment of the ω_n^{**} mode indicates the existence of a complex structure induced by the displacement which is influenced by the mixing of Bi^{3+} 6*s* electron with *d* orbital in the *B*-site ions. The splitting of phonon modes due to cation mass difference is also found in our data. The temperature dependence of resonant frequencies and damping coefficients confirms the decreasing of both the lattice constant and provides further confirmation of the orientational dipolar disorder in the bismuth pyrochlores.

ACKNOWLEDGMENTS

This work was supported in part by the NSF Condensed Matter Physics through Grant No. DMR-0305043 and the DOE through Grant No. DE-AI02-03ER46070.

[1] A. W. Sleight, Inorg. Chem. **7**, 1704 (1969).
[2] M. Lanagan, D. Anderson, A. Baker, J. Nino, S. Perini, C. A. Randall, T. R. Strout, T. Sogabe, and H. Youn, in *Proceedings of the International Symposium on Microelectronics*, edited by J. Graves (Baltimore, MD, 2001), p. 155.
[3] G. I. Golovshchikova, V. A. Isupov, A. G. Tutov, I. E. Mylnikova, P. A. Nikitnia, and O. I. Tulinova, Sov. Phys. Solid State **14**, 2539 (1973).
[4] G. Jeanne, G. Desgardin, and B. Raveau, Mater. Res. Bull. **9**, 1321 (1974).
[5] I. Levin, T. G. Amos, J. C. Nino, T. A. Vanderah, C. A. Randall, and M. T. Lanagan, J. Solid State Chem. **168**, 69 (2002).
[6] R. L. Withers, T. R. Welberry, A.-K. Larsson, Y. Liu, L. Noren, H. Rundlof, and F. J. Brink, J. Solid State Chem. **177**, 231 (2004).
[7] F. Brisse and O. Knop, Can. J. Chem. **48**, 859 (1968).
[8] R. A. McCauley, J. Opt. Soc. Am. **63**, 721 (1973).
[9] S. Kamba, V. Porokhonskyy, A. Pashkin, V. Bovtun, J. Petzelt, J. C. Nino, S. Trolier-McKinstry, M. T. Lanagan, and C. A. Randall, Phys. Rev. B **66**, 054106 (2002).
[10] J. C. Nino, M. T. Lanaguan, and C. A. Randall, Appl. Phys. Lett. **81**, 4404 (2002).
[11] J. C. Nino, M. T. Lanagan, and C. A. Randall, J. Mater. Res. **16**, 1460 (2001).
[12] J. C. Nino, Ph.D. thesis, The Pennsylvania State University, 2002.
[13] F. Wooten, *Optical Properties of Solids* (Academic Press, New York, 1972).
[14] A. L. Hector and S. B. Wiggin, J. Solid State Chem. **177**, 139 (2004).
[15] M. Avdeev, M. K. Hass, J. D. Jorgensen, and R. J. Cava, J. Solid State Chem. **169**, 24 (2002).
[16] R. D. Shannon, Acta Crystallogr., Sect. A: Cryst. Phys., Diffr., Theor. Gen. Crystallogr. **32**, 751 (1976).
[17] B. J. Kennedy, Mater. Res. Bull. **32**, 479 (1997).
[18] B. E. Scheetz and W. B. White, Opt. Eng. **22**, 302 (1983).
[19] R. J. Betsch and W. B. White, Spectrochim. Acta, Part A **34**, 505 (1978).